

Incommensurate structures and epitaxial growth of Li on Ru(0001): A quantitative low-energy electron-diffraction study

M. Gierer, H. Over, H. Bludau, and G. Ertl

Fritz-Haber-Institut der Max-Planck-Gesellschaft, Faradayweg 4-6, D-14195 Berlin, Germany

(Received 21 February 1995)

The structural properties of Li films on a Ru(0001) surface during initial growth were determined employing the technique of low-energy electron diffraction (LEED). For submonolayer coverages between $\Theta_{\text{Li}}=0.61$ and $\Theta_{\text{Li}}=0.78$, incommensurate structures oriented along high-symmetry directions of the substrate were observed. Fully dynamical LEED calculations of a (5×5) structure modeling the Li overlayer at $\Theta_{\text{Li}}=0.64$ revealed a Li-Ru interlayer spacing of $2.17 \pm 0.10 \text{ \AA}$. The computational effort for solving this structure could be significantly reduced by using a (5×1) unit mesh instead of the (5×5) unit cell without losing structural information. The first Li layer is completed at a coverage of 0.78. In the multilayer regime, the Ru(0001)-Li system exhibits also long-range order as indicated by adsorbate-induced hexagonal LEED patterns. LEED structure analyses of Li films with thicknesses of two and three layers revealed that the Li film is grown fcc(111)-like on Ru(0001). The interlayer spacings are $D_{\text{Li-Li}}=2.35 \pm 0.10 \text{ \AA}$ and $D_{\text{Li-Ru}}=2.35 \pm 0.10 \text{ \AA}$; the Li hard-sphere radius turns out to be $1.52 \pm 0.05 \text{ \AA}$, close to the metallic Pauling radius.

I. INTRODUCTION

Advancing our understanding of the growth of thin films on metal substrates is closely connected with the knowledge about the overlayer geometry during this process which, at least in principle, is accessible by low-energy electron diffraction (LEED) structural analyses if the adsorbate films exhibit sufficient long-range order. For thick adsorbate films (say, more than about eight layers), the structural analysis is simplified by the fact that the influence of the substrate on the $I(V)$ curves of the adsorbate-induced LEED spots becomes negligible owing to the small elastic mean free path of the electrons. Under these conditions, it is possible to calculate $I(V)$ curves of adsorbate-induced LEED spots using a (1×1) unit cell of the overlayer structure. In doing so, several ordered grown metal films have been quantitatively analyzed with LEED.¹⁻³ For a nine-monolayer-thick Mg film on Ru(0001), for example, a hexagonal LEED pattern aligned along the high-symmetry direction of Ru(0001) shows up, which is indicative of epitaxial growth, while the LEED spots of the Ru substrate have vanished. A LEED structural analysis revealed that Mg forms a Mg(0001) film with bulklike interlayer distances except for the topmost layer spacing, which was slightly expanded,³ consistent with a recent LEED analysis of a single-crystal Mg(0001) surface.⁴

In order to obtain information about the initial growth of metals on metals, one has to study thin adlayer films for which corresponding LEED $I(V)$ curves are strongly affected by the substrate due to multiple scattering. Several LEED structural analyses of complete metal monolayers grown on metal substrates have been reported, such as Cd on Ti (Ref. 5) and Fe on Ru(0001).⁶ All these systems are characterized by the persistence of a (1×1) LEED pattern upon evaporation of one monolayer of the adsorbate, consistent with pseudomorphic

growth of the first layer. Accordingly, the calculations could be easily performed due to the small size of the (1×1) unit cell.

In many cases, however, incommensurate structures, i.e., coincidence lattices or incoherent structures, appear near the completion of the first monolayer. These incommensurate structures are commonly modeled by relatively large unit cells in which the adatoms occupy inequivalent adsorption sites. LEED structural analyses may therefore become time consuming and cumbersome so that it is not surprising that only very few structural analyses of such systems have been reported, as, for example, with Ir(100)- (5×1) -Ir (Ref. 7) and Ru(0001)- (3×3) -Na.⁸ An approximation for treating incommensurate structures was recently proposed by Grünberg and Moritz,⁹ by which intralayer multiple scattering is treated correctly for an evenly dispersed adlayer, while modulations of the adlayer are taken into account kinematically. The coupling of the scattering matrices of the incommensurate layer to the substrate is performed within the framework of the beam set neglect method.¹⁰ In this contribution, we present a much simpler method of the analysis of incommensurate $(n \times n)$ structures by folding them back onto a $(n \times 1)$ unit cell. This approach is applied to the structural analysis of the Ru(0001)-Li surface at a Li coverage of 0.64 which is modeled by a (5×5) superstructure containing 16 Li atoms.

Ru(0001)-alkali-metal systems for submonolayer coverages have already been the subject of several LEED investigations (see, e.g., Refs. 8 and 11-18). In the submonolayer regime, repulsive interactions between the positively charged adparticles lead to the formation of evenly dispersed adlayers on the Ru(0001) surface as reflected by, among other factors, the formation of liquid-like ring structures at low coverages, and rotation or compression phases at higher coverages. For the Ru(0001)-Li system, Doering and Semancik¹¹ reported on

rotated structures for Li coverages of $\Theta=0.33-0.46$, which are metastable and transform, upon annealing, to structures that are oriented along high-symmetry directions of the substrate. The Li-monolayer coverage was determined to be $\Theta=0.46$, a value which is at odds with that found in this study. The tendency to occupy highly symmetric sites on the substrate surface, along with the dipole-dipole repulsion between the alkali-metal atoms, leads also to the formation of commensurate phases at certain coverages; on the Ru(0001) surface, a (2×2) phase at $\Theta=0.25$ and a $(\sqrt{3}\times\sqrt{3})R30^\circ$ structure at $\Theta=0.33$ have been observed with Li, Na, K, Rb, and Cs. With the exception of Ru(0001)- (2×2) -Li, these phases were the subject of LEED analyses.^{8,12-15} For the $(\sqrt{3}\times\sqrt{3})R30^\circ$ structure, all alkali-metal species reside in the threefold hcp site, while in the (2×2) phase, the alkali-metal atoms occupy threefold fcc sites, except for Cs, which sits in the onefold coordinated on-top position. For the Ru(0001)- $(\sqrt{3}\times\sqrt{3})R30^\circ$ -Li system, the Li-Ru interlayer distance was determined to be 2.25 ± 0.04 Å,¹⁵ equivalent to a Li hard-sphere radius of 1.39 Å, which is between the values for the covalent and the metallic Pauling radius of 1.23 and 1.55 Å.

For coverages exceeding one monolayer, information on the geometry of alkali atoms on Ru(0001) is still lacking. Ordered alkali-metal multilayers with a bcc(110) structure could be prepared for potassium on a Ni(100) surface, which was also the subject of a quantitative LEED analysis.² With the Ru(0001) surface, however, no ordered structure has been observed for multilayer films of Na, K, Rb, and Cs so that LEED was not suitable for providing much information on the local geometry in the course of the growth of these alkali-metal films. The absence of ordered multilayer structures may be related to the threefold $p3m1$ symmetry of the Ru(0001) substrate, which allows the coexistence of different domains of bcc(110) adsorbate structures, thus preventing the formation of thick monocrystalline adsorbate films. At this point, it is important to note that the Ni(100) surface used for the growth of the K multilayers (see Ref. 2) was slightly rippled, indicating the existence of steps that may break the fourfold symmetry and permit growth only in one orientation.

Unlike other alkali metals, Li on Ru(0001) exhibits long-range order in the multilayer regime at low temperatures (50 K) as evident from an adsorbate-induced hexagonal LEED pattern. The bulk properties of Li are qualitatively different from those of Na, K, Rb, and Cs in that Li transforms below 70 K partly into a hcp configuration; introducing stress, a fcc configuration can be formed.¹⁹ Both the fcc (111) and hcp(0001) surfaces exhibit the same symmetry as Ru(0001). This may enable the growth of adsorbate layers without losing the long-range order by the coexistence of different domains. Investigations of bulk Li with neutron diffraction at very low temperatures (4.2 K) indicated an even more complicated close-packed rhombohedral structure with stacking sequence *ABCBCACAB*.²⁰

In the following, we first describe results for the Ru(0001)-Li system obtained by LEED and thermal desorption spectroscopy (TDS) for coverages ranging

from submonolayers (we concentrate on coverages near the completion of the first Li monolayer) to multilayers. Next, we turn to LEED structural analyses of Li films consisting of one, two, and three adlayers, which supply detailed information on the adsorbate geometry during the initial stages of film growth of Li.

II. EXPERIMENT AND CALCULATIONS

The experiments were conducted in an ultrahigh-vacuum chamber. LEED measurements were carried out by using a four-grid optics, and $I(V)$ data were recorded using a computer-controlled video-LEED system.²¹ Lithium was evaporated from a well-outgassed SAES getter source. The coverage was determined by TDS and calibrated using the optimum $(\sqrt{3}\times\sqrt{3})R30^\circ$ structure, which was assumed to have a coverage of $\Theta=0.33$. Varying Li coverages in the submonolayer regime up to two monolayers were established by evaporation of Li multilayers and subsequent annealing in order to desorb excess Li. Li films with more than two layers were prepared directly by depositing a certain amount of Li at room temperature. For the LEED $I(V)$ measurements, the sample was cooled to 50 K. Further details about the experimental setup can be found in Refs. 12 and 22.

Fully dynamical LEED calculations were performed with the program package of Moritz.²³ Nine relativistically calculated phase shifts for Li and Ru were used; details about the computation of the phase shifts can be found elsewhere.²⁴ The agreement between calculated and measured $I(V)$ curves was quantified by using Pendry's r factor, r_p .²⁵

III. RESULTS AND DISCUSSION

The TD spectra shown in Fig. 1 exhibit, in accordance with the literature,^{11,26-28} a very broad feature in the submonolayer range, here labeled α , indicative of a strong decrease of the activation energy for desorption with increasing coverage. At coverages larger than $\Theta=0.78$, a sharp feature (β state) arises, and with further increase of the coverage above $\Theta=1.5$, a third peak γ appears (note that the coverage Θ is defined as the ratio of the densities of deposited Li atoms to Ru-substrate atoms). Similar TD spectra have been observed also for other alkali metals on Ru(0001), e.g., for cesium.¹² While the α peak corresponds to the desorption from the first Li layer, which is completed at a coverage of 0.78, the features β and γ can be attributed to the desorption from the second Li layer and from further Li layers, respectively.

A closer inspection of the TD spectra in Fig. 1 shows that the desorption peak of the second layer, i.e., the β peak, does not saturate for coverages up to about $\Theta=2$ for which certainly more than two Li layers are present on the surface. Assuming that the density within the completed second layer is similar to that in the first layer, the saturation coverage of the second layer should be about $\Theta=1.5$. The features β and γ are, however, not well separated in the TD spectra, indicating that desorption from the third layer still occurs at temperatures at

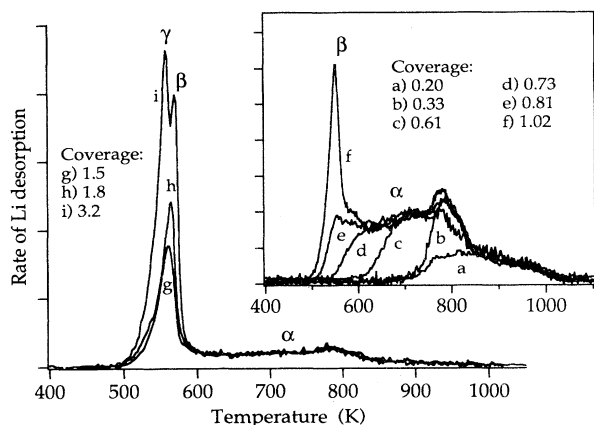


FIG. 1. TD spectra for the Ru(0001)-Li system; the heating rate was 5.4 K s^{-1} . Inset: TD spectra for low coverages (magnified four times).

which, for smaller initial coverages, the second layer would desorb. Calculations of Kreuzer *et al.*²⁹ revealed that with increasing initial coverage exceeding 2 ML, the β peak is shifted to higher temperatures, becomes narrower, and is enhanced in intensity, while the integral under the β peak is nearly constant. This behavior is due to the fact that the desorption from the second layer is inhibited as long as the third layer is still partly present.

A representative collection of LEED patterns taken at

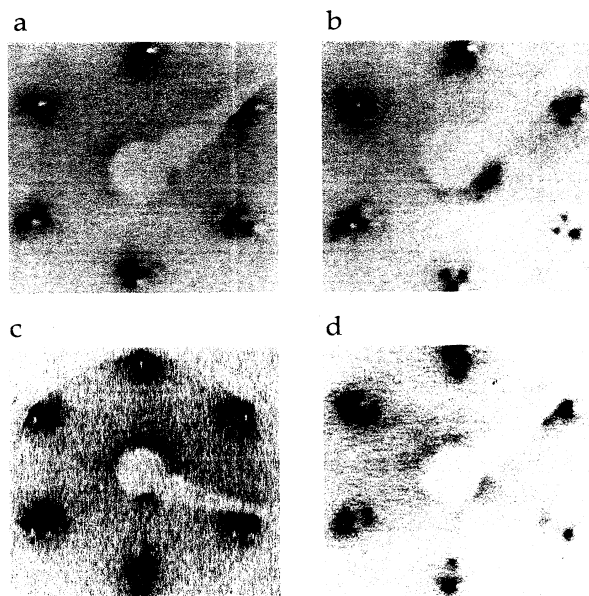


FIG. 2. LEED patterns before and after completion of the first Li monolayer (sample temperature = 50 K). The outer LEED spots correspond to the first integer-order beams, the inner spots are superstructure spots. (a) Incommensurate structure in the submonolayer regime ($\Theta=0.75$); (b) incommensurate structure ($\Theta=0.78$); this structure corresponds to one lithium monolayer. (c) $\Theta=1.02$; LEED spots appear roughly at the $(4/5, 0)$ position. (d) $\Theta=1.5$; the adsorbate-induced LEED spots at $(4/5, 0)$ persist upon further Li evaporation and indicate that long-range order exists even in the multilayer range.

$T=50 \text{ K}$ during the growth of Li films on Ru(0001) is depicted in Fig. 2. At $\Theta=0.33$, an ordered $(\sqrt{3} \times \sqrt{3})R 30^\circ$ structure appeared (not shown). At coverages higher than 0.61, incommensurate structures appeared with superstructure spots moving radially towards the substrate spots with increasing coverage [cf. Fig. 2(a)]. This is also shown in a series of profiles (Fig. 3), which is indicative of a continuously compressed, hexagonal Li overlayer oriented along the high-symmetry directions of the substrate, thus indicating epitaxial growth. For these phases, the local coverage is derived from the spot positions in the LEED pattern using the formula

$$\Theta = a_{\text{Li}}^2 / a_{\text{Ru}}^2 ;$$

$a_{\text{Li}}/a_{\text{Ru}}$ is the length of the reciprocal lattice vectors of the Li adlayer relative to that of the Ru substrate as given by the positions of the dominant superstructure spots and the substrate first-order spots. For the compression phases with $\Theta=0.61-0.78$, the local coverages according to the LEED patterns equal the global coverages as determined by TDS within an uncertainty of 0.01, thus indicating that the Li atoms are evenly distributed across the surface.

The LEED pattern at a coverage of $\Theta=0.78$ is depicted in Fig. 2(b). The Li adlayer is slightly rotated away from the high-symmetry directions of the substrate as indicated by the splitting of the superstructure LEED spots. At this coverage, the compression of the Li adlayer is finished, and the first Li monolayer is completed. For higher coverages, the sharp β peak arises in TDS, which is assigned to desorption from the second layer.

The found monolayer coverage of $\Theta=0.78$ is at variance with the value of 0.46 found by Doering and Semanick.¹¹ It compares well, however, with the trend found

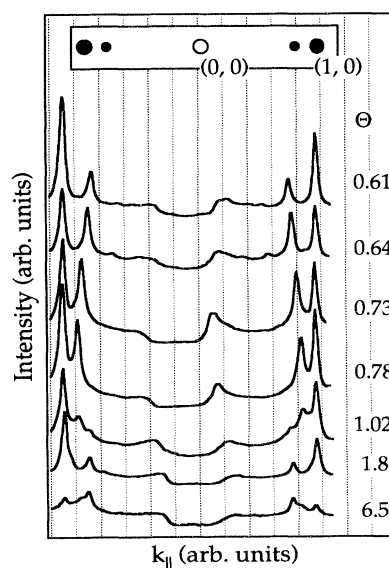


FIG. 3. LEED profiles for Li coverages between $\Theta=0.61$ and 6.5. For coverages in the submonolayer range ($\Theta=0.61-0.78$), compressed structures appear, while for $\Theta>0.78$, new spots arise that indicate long-range order also for Li multilayers.

TABLE I. Monolayer coverages, corresponding nearest-neighbor spacings d_{nn} , bulk values for the nearest-neighbor distances, and bulk moduli for alkali metals adsorbed on Ru(0001).

| Akali metal | Monolayer coverage | d_{nn} (Å) | d_{nn} (bulk) (Å) | Bulk modulus | Ref. |
|-------------|--------------------|--------------|--------------------------|---|-----------|
| Li | 0.78 | 3.06 | 3.01 (bcc) 3.11 (hcp) | 0.116×10^{11} N/m ² | This work |
| Na | 0.57 | 3.58 | 3.659 | 0.068×10^{11} N/m ² | 8 |
| K | 0.37 | 4.45 | 4.525 | 0.032×10^{11} N/m ² | 17 |
| Rb | 0.33 | 4.69 | 4.837 | 0.031×10^{11} N/m ² | 14 |
| Cs | 0.33 | 4.69 | 5.235 | 0.020×10^{11} N/m ² | 18 |

with other alkali metals on Ru(0001). In Table I, the monolayer coverages determined for Li, Na,¹⁶ K,¹⁷ Rb,¹⁴ and Cs (Ref. 18) are compiled along with the corresponding nearest-neighbor distances, which were calculated from the monolayer coverage under the assumption of an evenly dispersed alkali-metal layer on the surface. It can be seen that the interatomic distance of Li of 3.06 ± 0.04 Å is equal to the bulk values for bcc and hcp Li within the error bars. The Na and K monolayers on Ru(0001) are slightly contracted, while the monolayers of Rb and Cs are strongly compressed. This tendency is paralleled by the bulk moduli (also included in Table I), which decrease when going from Li to Cs; the smaller the bulk modulus, the “softer” a metal and the smaller the amount of energy required to compress the adlayer. The contraction of the Rb and Cs layers is also indicative of a strong adsorbate-substrate interaction allowing a higher density of alkali-metal atoms on the Ru surface than in the bulk alkali materials.

At coverages above one monolayer, superstructure spots show up on the LEED screen near the (4/5,0) position, as shown in Fig. 2(c) for $\Theta = 1.02$. This hexagonal LEED pattern remains visible also for higher coverages in the multilayer range while the split LEED spots of the first monolayer vanish [Fig. 2(d)]. From the positions of the adsorbate-induced LEED spots, a lateral lattice constant of 3.34 ± 0.04 Å can be derived. This value is larger than the lattice constant of 3.06 Å obtained for the case of one monolayer. The lower density within the first ad-

layer of this phase suggests a mass transport of Li atoms from the first into the second layer.

In order to obtain information about the local geometry in the Li films, we measured LEED $I(V)$ curves of the dominant superstructure spots near the (4/5,0) position for various Li coverages ranging from $\Theta = 0.64$ to 3.2. It was not possible to measure $I(V)$ curves of other adsorbate-induced spots, which may be a consequence of some disorder in the adlayers or of the weak scattering power of lithium. Figure 4 demonstrates that the $I(V)$ curve at $\Theta = 0.64$ is substantially different from the $I(V)$ curve of the same spot observed at $\Theta = 1.5$ (about two Li layers). In the TD spectra, at this coverage the β peak is developed (cf. Fig. 1). Increasing the Li coverage further, the γ peak arises in the TD spectra, again accompanied by pronounced changes in the $I(V)$ curves.

Fully dynamical LEED calculations were performed for Li films with coverages of $\Theta = 0.64$, 1.5, and 3.2. First, we turn to the submonolayer with a coverage of $\Theta = 0.64$, which can be described as a (5×5) structure; in the corresponding profile displayed in Fig. 3, weak intensities associated with the second- and third-order beam can be discerned. The fourth-order spot is, however, much more intense, consistent with an evenly dispersed Li adlayer (coincidence lattice). The (5×5) unit mesh contains 16 Li atoms, making the computation of $I(V)$ spectra very time consuming. A simple method to circumvent this difficulty is to perform the calculations with a (5×1) unit mesh instead of the (5×5) cell; see Fig. 5(a). With only four Li atoms, this is the smallest unit cell, which is able to generate the (4/5,0) LEED spot. For this beam, we calculated $I(V)$ spectra for various Li-Ru interlayer spacings. Optimum agreement between theory and experiment was achieved with a Li-Ru interlayer spacing of 2.17 ± 0.10 Å, which agrees within the error bars with the spacing 2.25 ± 0.05 Å as determined for the $(\sqrt{3} \times \sqrt{3})R30^\circ$ phase;¹⁵ the experimental intensities are compared with calculated ones in Fig. 5(b).

In order to test the accuracy of the approximation applied above, the calculations were alternatively carried out with the full (5×5) configuration, which exhibits $p3m1$ symmetry; see Fig. 6(a). In the LEED program, symmetries are extensively exploited in order to reduce the computing time.²³ The calculations with the (5×5) unit cell revealed the same result for the Li-Ru interlayer spacings as the calculations with the (5×1) mesh as shown in the r -factor plot in Fig. 6(c). A comparison of the calculated $I(V)$ curves shown in Fig. 6(b) demon-

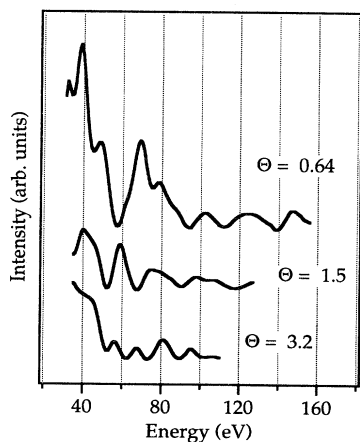


FIG. 4. $I(V)$ curves for the adsorbate-induced LEED spots for Li coverages of $\Theta = 0.64$, 1.5, and 3.2.

strates that the peak positions are nearly identical. Although in this case the exploitation of the symmetry allows one to perform the calculations with the full (5×5) unit cell, generally, the computation with the $(n \times 1)$ unit mesh instead of a $(n \times n)$ unit cell has some advantages: First, this approximation enables the analyses of incommensurate structures also with LEED programs that do not exploit the symmetry of the structure so as to reduce

the computation time. Second, with increasing values of n , the number of atoms and the number of beams to be taken into account for the computation of the superstructure scattering matrix, and consequently the computing time, rises much more rapidly for the $(n \times n)$ unit cell than for the $(n \times 1)$ mesh.

A comparison of the (5×1) and the (5×5) configurations shown in Fig. 5(a) and Fig. 6(a) reveals also that the specific adsorption sites of the Li atoms are quite different: While in the (5×1) cell chosen for the calculations, all Li atoms reside near threefold or bridge

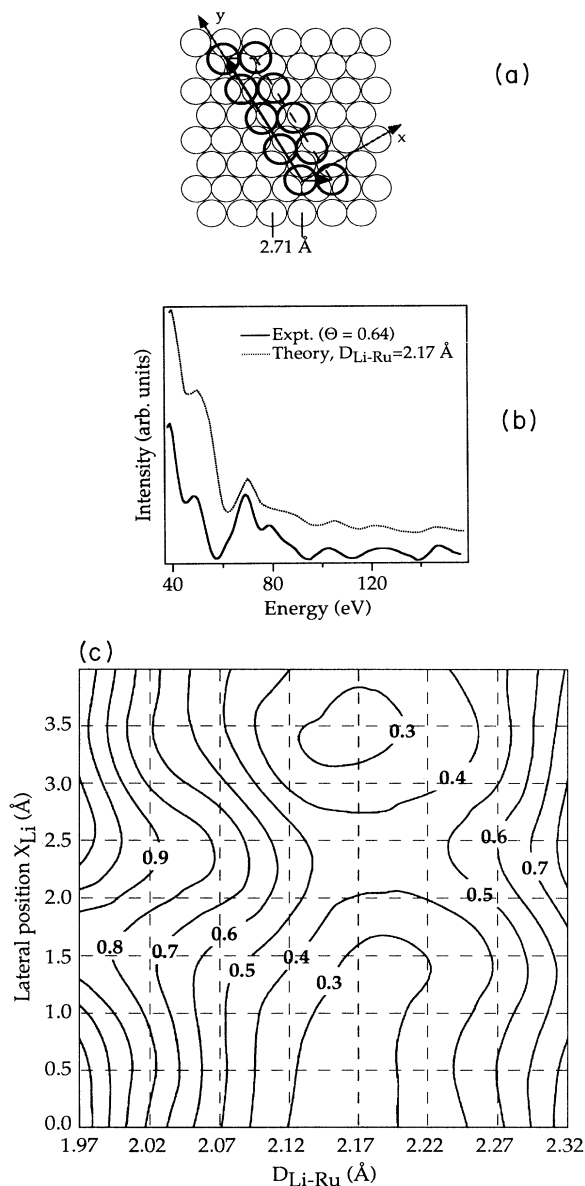


FIG. 5. (a) Geometry of the (5×1) cell, which was chosen for the calculation of $I(V)$ curves of the $(4/5,0)$ beam of the $\text{Ru}(0001)$ - (5×5) -Li structure. This cell is the smallest one generating the $(4/5,0)$ spot in the LEED pattern. (b) Measured and calculated $I(V)$ curves for $\Theta = 0.64$; the calculations were carried out with a (5×1) unit mesh and a flat adsorbate layer with a Li-Ru interlayer spacing of $D_{\text{Li-Ru}} = 2.17 \text{ \AA}$. The optimum Pendry r factor is $r_p = 0.27$. (c) r_p factor as a function of the Li-Ru interlayer spacing and the lateral registry along the line x shown in (a).

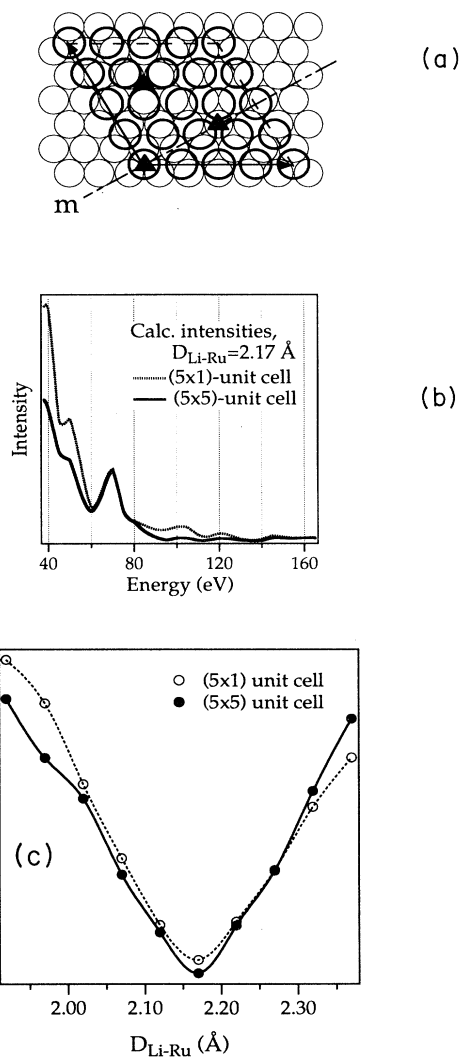


FIG. 6. (a) Geometry of the (5×5) cell chosen for the calculation of $I(V)$ curves of the $(4/5,0)$ beam of the $\text{Ru}(0001)$ - (5×5) -Li structure. The $p3m1$ symmetry of the structure leads to five symmetrically inequivalent Li atoms in the unit cell; a mirror plane (dash-dotted line) and threefold-rotational axes (shaded triangles) are indicated. (b) Comparison of the $I(V)$ curves calculated with the geometries shown in Fig. 5(a) and in (a); Li-Ru interlayer spacing $D_{\text{Li-Ru}} = 2.17 \text{ \AA}$. (c) r_p factor as a function of the Li-Ru interlayer spacing $D_{\text{Li-Ru}}$ for the (5×1) and (5×5) geometries as shown in Fig. 5(a) and in (a).

sites, in the (5×5) configuration also positions near on-top sites are occupied. The similarity of the respective $I(V)$ curves [cf. Fig. 6(b)] indicates, however, that the lateral positions of the Li atoms have only minor influence on the intensities. At this point, it is important to note that for the calculation of the scattering matrix of the adsorbate layer, a sum over the Li atoms (multiplied with a phase factor) is performed³⁰ which corresponds to some kind of averaging process over different Li adgeometries. This "average" will presumably not alter when the Li layer is shifted parallel to the surface. In order to further estimate the influence of the Li adsorption sites on the $I(V)$ curves and on the optimized Li-Ru interlayer spacing, we carried out calculations for various (5×1) configurations which are shifted along the line x as indicated in Fig. 5(a). The r_p -factor dependence on the lateral shift and the Li-Ru interlayer spacing is shown in Fig. 5(c) and demonstrates that the optimum layer spacing is not affected by the lateral positions of the Li atoms and that r_p is not that sensitive to the lateral positions of the Li atoms.

Other parameters that may exert influence on the $I(V)$ curves are vertical and lateral modulations within the adlayer. Let us first consider diffraction spots of the reciprocal lattice of the evenly dispersed adlayer, which are present in the kinematic limit [for example, the $(4/5, 0)$ spot of Ru(0001)- (5×5) -Li]. Modulations of the lithium layer may have a similar effect on these particular LEED spots as thermal disorder and hence may be approximated by a certain Debye temperature. The larger the modulation amplitudes, the lower the value of the Debye temperature of the adatoms to be chosen for the optimum configuration. This consideration, however, does not hold for adsorbate-induced LEED spots which are not associated with the reciprocal lattice of the evenly dispersed adlayer: With the introduction of modulations in the adlayer, the intensity of these spots increases (at least in the kinematic limit). For the Ru(0001)- (5×5) -Li phase, a lowering of the Debye temperature below the value of 400 K as determined for the Ru(0001)- $(\sqrt{3} \times \sqrt{3})R 30^\circ$ structure¹⁵ did not improve the r_p factor. We therefore think that the Li adlayer is not strongly modulated.

At this point, it is instructive to compare the results of this analysis with those of a structural analysis of the Ru(0001)- (3×3) -Na system for which a comparatively large data set, containing five fractional-order and three integer-order beams, was available.⁸ Despite the appreciable size of this data set, the adsites of the Na atoms could not be determined unambiguously, which may be traced back to the "averaging" effect mentioned above. Furthermore, the LEED analysis of the Ru(0001)- (3×3) -Na system revealed that the $I(V)$ curves were not sensitive to a vertical buckling within the Na layer as long as these values do not exceed 0.2 Å. Similar to the Ru(0001)- (5×5) -Li phase, the only parameter that could be determined with high confidence was the Na-Ru interlayer spacing.

Next, we turn to calculations for the $I(V)$ curves measured in the multilayer range and begin with the coverage $\Theta = 1.5$ corresponding to about two Li layers. The lateral lattice constant of 3.34 ± 0.04 Å derived from the intensity profiles is close to the interatomic spacing of 3.38 Å

when Li atoms are arranged in a (5×5) coincidence lattice. Therefore, the calculations have been carried out using a (5×5) unit mesh with two Li layers. A variation of the Li-Li and the Li-Ru interlayer spacings within a grid search led to optimum layer spacings of $D_{\text{Li-Ru}} =$

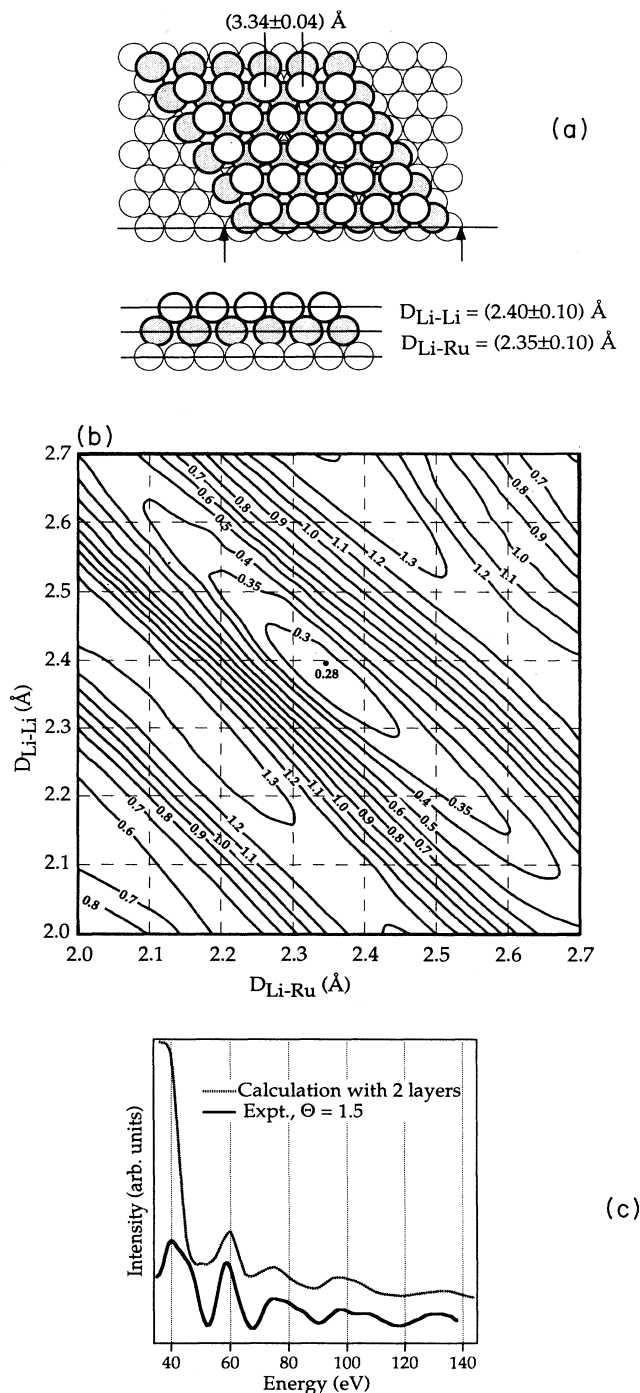


FIG. 7. (a) Optimum geometry of the ordered Ru(0001)-Li structure ($\Theta = 1.5$). (b) r_p geometry in dependence on the Li-Ru and the Li-Li interlayer spacing $D_{\text{Li-Ru}}$ and $D_{\text{Li-Li}}$. (c) $I(V)$ curves for the optimum geometry shown in (a) (Pendry r factor $r_p = 0.28$).

TABLE II. Intralayer spacing and interlayer spacing for Li-bulk structures in comparison with the ordered Ru(0001)-Li structure at $\Theta=3.2$.

| | bcc(111) | fcc(111) | hcp(0001) | Ru(0001)-Li |
|--------------------|----------|----------|-----------|-------------|
| Intralayer spacing | 4.91 Å | 3.11 Å | 3.11 Å | 3.34±0.04 Å |
| Interlayer spacing | 2.00 Å | 2.55 Å | 2.55 Å | 2.40±0.10 Å |

2.35±0.10 Å and $D_{\text{Li-Li}}=2.40\pm0.10$ Å and a final agreement between theory and experiment of $r_p=0.28$; the optimum geometry is shown in Fig. 7(a). The corresponding r -factor plot in Fig. 7(b) demonstrates that the (4/5,0) beam is sufficiently sensitive to determine these parameters accurately. The $I(V)$ curves for the optimum configuration are displayed in Fig. 7(c). Calculations were also performed with one and three adlayers; however, these geometries can clearly be excluded on the basis of corresponding r -factor values of $r_p > 0.5$. Therefore, we conclude that the ordered part of the Li film consists of two Li layers.

As mentioned above, Li exists, in contrast to the other alkali metals, not only in a bcc but also in hcp or fcc configurations at low temperatures. As a consequence, three surfaces of bulk Li leading to a hexagonal LEED pattern are conceivable: hcp(0001), fcc(111), and bcc(111). The close-packed bcc surface, bcc(110), would, on the other hand, give rise to the appearance of additional LEED spots as observed, for example, for the ordered multilayer growth of Fe on Ru(0001) (Ref. 6) but not observed with Li on Ru(0001).

The Li-Li interlayer spacing of the Li film on Ru(0001) is compared with corresponding values of the hexagonal bulk surfaces in Table II. This comparison reveals that the Li film is substantially distorted by the presence of the Ru substrate and certainly cannot be interpreted as a Li-bcc(111) surface. It seems, therefore, to be plausible to compare the two-layer lithium film on Ru(0001) with either a distorted hcp(0001) or a distorted fcc(111) phase. Closer inspection of Table II shows that for the Ru(0001)-Li phase the intralayer distances within the adsorbate layers are larger, and the interlayer distance from the second to the first adlayer is smaller than in the fcc(111)-Li and hcp(0001)-Li modifications. This deformation of the Li film may result from an attractive interaction between the Li atoms in the second adlayer and the Ru atoms of the topmost substrate layer which may

TABLE III. Optimum Pendry r factors and Li-Li interlayer spacings for three and four Li layers on Ru(0001) exhibiting fcc and hcp stacking sequences. $I(V)$ curves were measured at $\Theta=3.2$; Li-Ru interlayer spacing $D_{\text{Li-Ru}}=2.35$ Å.

| | $D_{\text{Li-Li}}$ | r_p |
|---------------|--------------------|-------|
| 3 layers, fcc | 2.35 Å | 0.26 |
| 3 layers, hcp | 2.40 Å | 0.48 |
| 4 layers, fcc | 2.35 Å | 0.57 |
| 4 layers, hcp | 2.45 Å | 0.81 |

also account for the higher desorption temperature of the second-layer compared to Li multilayers in TDS.

With two Li layers it is not possible to discriminate between a fcc(111)- or hcp(0001)-like growth of Li; note that the stacking sequence is $ABAB\dots$ for an hcp(0001) surface and $ABCABCABC\dots$ for an fcc(111) surface so that at least three adlayers are needed to assign the surface type unambiguously. To this end, we analyzed the $I(V)$ curves measured at $\Theta=3.2$ and performed fully dynamical calculations of Ru(0001)-(5×5)-Li with three and four layers. The Li-Li and Li-Ru interlayer spacings within an fcc(111) or hcp(0001) geometry were varied between 2.2 and 2.6 Å (i.e., near the values of $D_{\text{Li-Ru}}=2.35$ Å and $D_{\text{Li-Li}}=2.40$ Å, as determined for the ordered structure at $\Theta=1.5$). Best agreement with experiment was achieved with a three-layer fcc(111) configuration exhibiting interlayer spacings of $D_{\text{Li-Ru}}=2.35\pm0.10$ Å and $D_{\text{Li-Li}}=2.35\pm0.10$ Å ($r_p=0.26$). The nearest-neighbor distance between Li atoms in the second and the third layers is 3.04 ± 0.10 Å, corresponding to a Li hard-sphere radius of 1.52 ± 0.05 Å, which is close to the metallic Pauling radius (1.55 Å). Other possible arrangements could clearly be ruled out on the basis of corresponding r factors as compiled in Table III. The comparison of the $I(V)$ curves calculated for three adlayers with the experiment shows that the fcc(111) configuration leads to a significantly better agreement than the hcp(0001) structure, especially for higher energies of the incident electrons (cf. Fig. 8). The appearance of the fcc(111) lithium film is quite interesting because fcc-Li exists in the bulk only at low temperatures in combination with an applied stress. The latter condition appears to be realized for the Li films by the attractive interaction of the substrate with the lithium layers.

With further Li deposition beyond four monolayers, the long-range order of the adlayers becomes poorer. The intensity between the first-order spots of the adsorbate and the substrate, which can be seen in the profile for $\Theta=6.5$ in Fig. 3, indicates that part of the ordered structure (presumably the top layers) exhibits smaller in-

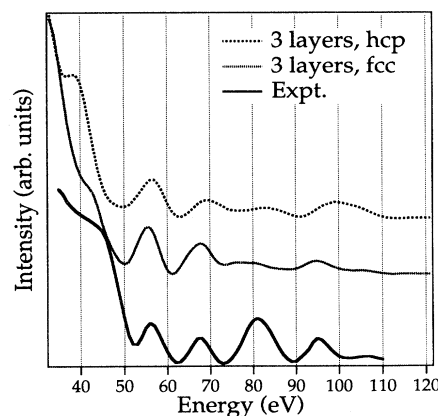


FIG. 8. $I(V)$ curves calculated for three Li layers on Ru(0001) (for interlayer spacings see Table III) in comparison with the experimental curve recorded at $\Theta=3.2$. The fcc(111) configuration reveals a much better Pendry r factor ($r_p=0.26$) than the hcp(0001) geometry ($r_p=0.48$).

tralayer spacings; this behavior is plausible because the intralayer distance of $3.34 \pm 0.04 \text{ \AA}$ as determined for the two- and three-layer films is larger than the corresponding lithium bulk values, which was explained by an attractive interaction between the Li atoms in the second layer with the substrate. For higher coverages, this interaction may have only minor influence on the top lithium layers, for which then the tendency to take bulklike intralayer spacings may become dominant. The measurement of reliable $I(V)$ data in this coverage range is, however, difficult since the background correction becomes problematic.

Because the chemistry of lithium and magnesium exhibits some similarities,³¹ it is instructive to compare the Ru(0001)-Li system with the Ru(0001)-Mg system. Mg crystallizes, like ruthenium, in an hcp configuration. Similar to Li, for Mg submonolayer coverages between 0.65 and 0.75, a continuous compression of the Mg overlayer takes place.³ Long-range order persisted also upon further evaporation, and a well-ordered hexagonal LEED pattern was observed for high coverages in the multilayer range, for which a LEED analysis revealed that the atomic arrangement corresponds to the Mg(0001) bulk geometry. In contrast to the Ru(0001)-Mg system, in which Mg builds up its bulk structure, the long-range order in the Ru(0001)-Li system becomes very poor with increasing coverage; this may be due to the fact that the first Li adlayers grown on Ru(0001) are strained by the substrate. This behavior is also known for pseudomorphic grown metal films on metal substrates: When the film exceeds a certain thickness, the substrate-induced strain

is relieved by the formation of misfit dislocations, thus destroying the long-range order. At this point, it is important to note that at low temperatures the order of lithium-bulk material is also poor due to the coexistence of hcp, fcc, and bcc structures.

In summary, it could be demonstrated that LEED is a very powerful method for obtaining information on the adsorbate geometry during the initial growth of metal films on metal substrates even if the adsorbate forms incommensurate structures. With the system Ru(0001)-Li, the first order of the adsorbate-induced LEED spots contains enough information to determine the Li-Li and Li-Ru interlayer spacings with confidence. For incommensurate phases in the submonolayer range, the Li-Ru layer spacing amounts to $2.17 \pm 0.10 \text{ \AA}$ for the Ru(0001)-(5×5)-Li structure. The first lithium layer is completed at a coverage of $\Theta = 0.78$. Analyses of ordered structures with two and three Li layers revealed that Li builds up an fcc(111)-like stacking sequence with a lattice constant of $3.34 \pm 0.04 \text{ \AA}$ and interlayer spacings of $D_{\text{Li-Ru}} = 2.35 \pm 0.10 \text{ \AA}$ and $D_{\text{Li-Li}} = 2.35 \pm 0.10 \text{ \AA}$, respectively. The Li film is distorted by the Ru substrate, as indicated by a smaller value for the Li-Li interlayer spacing together with a larger lattice constant if compared with the pure fcc(111)-Li surface. This distortion may indicate an attractive interaction between the Li atoms in the second adsorbate layer and the Ru substrate.

ACKNOWLEDGMENT

We thank H. J. Kreuzer for fruitful discussions about the interpretation of the TD spectra.

- ¹F. Jona and P. M. Marcus, in *Surface Physics and Related Topics*, edited by F. J. Yang, G. J. Ni, X. Wang, K. M. Zhang, and D. Lu (World Scientific, Singapore, 1990), p. 213, and references therein.
- ²B. S. Itchkawitz, A. P. Baddorf, H. L. Davis, and E. W. Plummer, *Phys. Rev. Lett.* **68**, 2488 (1992).
- ³H. Over, T. Hertel, H. Bludau, S. Pflanz, and G. Ertl, *Phys. Rev. B* **48**, 5572 (1993).
- ⁴P. T. Sprunger, K. Pohl, H. L. Davis, and E. W. Plummer, *Surf. Sci.* **297**, L48 (1993).
- ⁵H. D. Shih, F. Jona, D. W. Jepsen, and P. M. Marcus, *Phys. Rev. B* **15**, 5550 (1977).
- ⁶D. Tian, H. Li, F. Jona, and P. M. Marcus, *Solid State Commun.* **80**, 783 (1991).
- ⁷W. Moritz, F. Müller, D. Wolf, and H. Jagodzinski, in *Proceedings of the 9th Vacuum Congress and 5th International Conference on Solid Surfaces, Madrid, 1983* (American Nuclear Society, La Grange Park, IL, 1983), p. 70.
- ⁸T. Hertel, H. Over, H. Bludau, M. Gierer, and G. Ertl, *Surf. Sci.* **301**, 1 (1994).
- ⁹T. Grünberg and W. Moritz (unpublished).
- ¹⁰M. A. Van Hove, Rongfu Lin, and G. A. Somorjai, *Phys. Rev. Lett.* **51**, 778 (1983).
- ¹¹D. L. Doering and S. Semancik, *Surf. Sci.* **175**, L730 (1986).
- ¹²H. Over, H. Bludau, M. Skottke-Klein, G. Ertl, W. Moritz, and C. T. Campbell, *Phys. Rev. B* **45**, 8638 (1992).
- ¹³M. Gierer, H. Bludau, H. Over, T. Hertel, W. Moritz, and G. Ertl, *Surf. Sci.* **279**, L170 (1992).
- ¹⁴T. Hertel, H. Over, H. Bludau, M. Gierer, and G. Ertl, *Phys. Rev. B* **50**, 8126 (1994).
- ¹⁵M. Gierer, H. Over, H. Bludau, and G. Ertl, *Surf. Sci.* (to be published).
- ¹⁶L. Doering and S. Semancik, *Phys. Rev. Lett.* **53**, 66 (1984).
- ¹⁷R. Duszak and K. H. Prince, *Surf. Sci.* **205**, 143 (1988).
- ¹⁸J. Hrbek, *Surf. Sci.* **164**, 139 (1985).
- ¹⁹W. B. Pearson, *A Handbook of Lattice Spacings and Structures of Metals and Alloys* (Pergamon, London, 1985); *Gmelins Handbuch der Anorganischen Chemie; Lithium-Ergänzungband* (Verlag Chemie, Weinheim, 1960).
- ²⁰A. W. Overhauser, *Phys. Rev. Lett.* **53**, 64 (1984); C. M. McCarthy, C. W. Thompson, and S. A. Werner, *Phys. Rev. B* **22**, 574 (1980).
- ²¹D. von Gemünden, Doctoral thesis, Universität Erlangen-Nürnberg, 1990.
- ²²H. Bludau, Doctoral thesis, Freie Universität Berlin, 1992.
- ²³W. Moritz, *J. Phys. C* **17**, 353 (1983).
- ²⁴R. Feder and W. Moritz, *Surf. Sci.* **77**, 505 (1978).
- ²⁵J. B. Pendry, *J. Phys. C* **13**, 937 (1980).
- ²⁶J. A. Rodriguez, J. Hrbek, Y. W. Yang, M. Kuhn, and T. K. Sham, *Surf. Sci.* **293**, 260 (1993).
- ²⁷H. J. Jänsch, C. Huang, A. Ludviksson, and R. M. Martin, *Surf. Sci.* **315**, 9 (1994).
- ²⁸T. Greber, K. Freihube, R. Grobecker, A. Böttcher, K. Hermann, and G. Ertl, *Phys. Rev. B* **50**, 8755 (1994).
- ²⁹H. J. Kreuzer *et al.* (private communication).
- ³⁰M. A. Van Hove and S. Y. Tong, *Surface Crystallography by LEED*, Springer Series in Chemical Physics Vol. 2 (Springer, Berlin, 1979).
- ³¹F. A. Cotton and G. Wilkinson, *Advance Inorganic Chemistry*, 5th ed. (Wiley, New York, 1988).

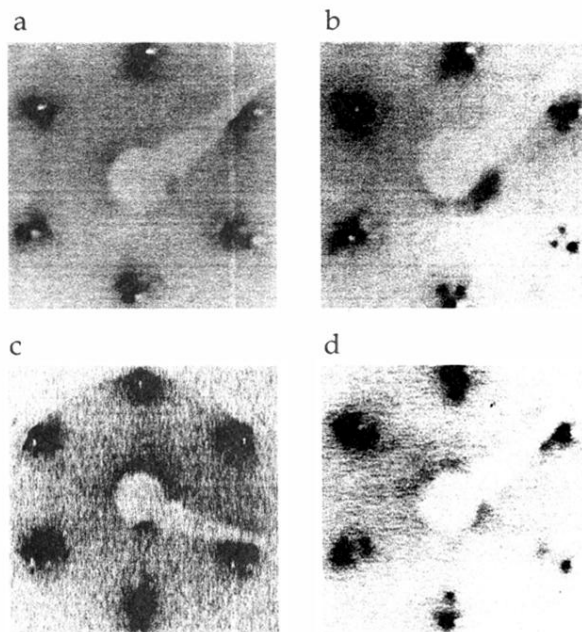


FIG. 2. LEED patterns before and after completion of the first Li monolayer (sample temperature = 50 K). The outer LEED spots correspond to the first integer-order beams, the inner spots are superstructure spots. (a) Incommensurate structure in the submonolayer regime ($\Theta=0.75$); (b) incommensurate structure ($\Theta=0.78$); this structure corresponds to one lithium monolayer. (c) $\Theta=1.02$; LEED spots appear roughly at the $(4/5,0)$ position. (d) $\Theta=1.5$; the adsorbate-induced LEED spots at $(4/5,0)$ persist upon further Li evaporation and indicate that long-range order exists even in the multilayer range.